Broadband behavior of transmission volume holographic optical elements for solar concentration

Paula Bañares-Palacios,[1] Samuel Álvarez-Álvarez,[1] Julia Marín-Sáez,[2] María-Victoria Collados,[1] Daniel Chemisana,[2] and Jesús Atencia[1,*]

[1]*Departamento de Física Aplicada, Instituto de Investigación en Ingeniería de Aragón (I3A), Universidad de Zaragoza, Facultad de Ciencias, Pedro Cerbuna 12, 50009 Zaragoza, Spain*

[2]*Departamento de Medio Ambiente (Sección de Física Aplicada), Universidad de Lleida, Escuela Politécnica Superior (INSPIRES), Jaume II 69, 25001 Lleida, Spain*

[*]*atencia@unizar.es*

Abstract: A ray tracing algorithm is developed to analyze the energy performance of transmission and phase volume holographic lenses that operate with broadband illumination. The agreement between the experimental data and the theoretical treatment has been tested. The model has been applied to analyze the optimum recording geometry for solar concentration applications.

© 2015 Optical Society of America

OCIS codes: (090.2890) Holographic optical elements; (090.7330) Volume gratings; (220.4298) Nonimaging optics; (350.6050) Solar energy.

References and links

1. D. Zhang, J. M. Castro, and R. K. Kostuk, "One-axis tracking holographic planar concentrator systems," J. Photonics Energy **1**(1), 015505 (2011).
2. R. K. Kostuk and G. Rosenberg, "Analysis and design of holographic solar concentrators," Proc. SPIE **7043**, 70430I (2008).
3. D. Zhang, M. Gordon, J. M. Russo, S. Vorndran, and R. K. Kostuk, "Spectrum-splitting photovoltaic system using transmission holographic lenses," J. Photonics Energy **3**(1), 034597 (2013).
4. J. E. Ludman, "Holographic solar concentrator," Appl. Opt. **21**(17), 3057–3058 (1982).
5. K. Froehlich, E. U. Wagemann, H. Schulat, H. Schuette, and C. G. Stojanoff, "Fabrication and test of a holographic concentrator for two color PV-operation," Proc. SPIE **2255**, 812–821 (1994).
6. J. E. Ludman, J. Riccobono, I. V. Semenova, N. O. Reinhand, W. Tai, X. Li, G. Syphers, E. Rallis, G. Sliker, and J. Martin, "The optimization of a holographic system for solar power generation," Sol. Energy **60**(1), 1–9 (1997).
7. M. Gordon, D. Zhang, S. Vorndran, J. M. Russo, C. K. Luscombe, S. E. Shaheen, and R. K. Kostuk, "Planar holographic spectrum-splitting PV module design," Proc. SPIE **8468**, 846808 (2012).
8. D. Chemisana, M. V. Collados, M. Quintanilla, and J. Atencia, "Holographic lenses for building integrated concentrating photovoltaics," Appl. Energy **110**, 227–235 (2013).
9. J. M. Castro, D. Zhang, B. Myer, and R. K. Kostuk, "Energy collection efficiency of holographic planar solar concentrators," Appl. Opt. **49**(5), 858–870 (2010).
10. Y. W. Zhang, C. S. Ih, H. F. Yan, and M. J. Chang, "Photovoltaic concentrator using a holographic optical element," Appl. Opt. **27**(16), 3556–3560 (1988).
11. Y. Luo, J. Castro, J. K. Barton, R. K. Kostuk, and G. Barbastathis, "Simulations and experiments of aperiodic and multiplexed gratings in volume holographic imaging systems," Opt. Express **18**(18), 19273–19285 (2010).
12. H. Kogelnik, "Coupled wave theory for thick hologram gratings," Bell Syst. Tech. J. **48**(9), 2909–2947 (1969).
13. R. R. A. Syms, "Vector effects in holographic optical elements," Opt. Acta (Lond.) **32**(11), 1413–1425 (1985).
14. A. M. López, M. P. Arroyo, and M. Quintanilla, "Some polarization effects in holographic volume gratings," J. Opt. A, Pure Appl. Opt. **1**(3), 378–385 (1999).
15. J. N. Latta, "Computer-based analysis of holography using ray tracing," Appl. Opt. **10**(12), 2698–2710 (1971).
16. A. Villamarín, J. Atencia, M. V. Collados, and M. Quintanilla, "Characterization of transmission volume holographic gratings recorded in Slavich PFG04 dichromated gelatin plates," Appl. Opt. **48**(22), 4348–4353 (2009).
17. R. Leutz and A. Suzuki, *Nonimaging Fresnel Lenses. Design and Performance of Solar Concentrators* (Springer-Verlag 2001).

#234591 - $15.00 USD Received 17 Feb 2015; revised 17 Apr 2015; accepted 20 Apr 2015; published 18 May 2015

1. Introduction

During the last years, designs of devices with holographic optical elements have been proposed to be used as solar concentrators. These designs include volume transmission phase holograms [1,2], mainly spherical lenses [3–5] and cylindrical lenses [6–8]. Precisely, the last ones are the most commonly suggested to avoid tracking in one direction. This type of holograms is used due to its high efficiency and low cost; however, it has two special characteristics that can affect its performance as solar concentrator: angular selectivity and chromatic selectivity.

Due to the angular selectivity, volume holograms have high efficiency only for a range of incidence directions that depends on the holographic material thickness and the interbeam angle at the recording step. Angular selectivity is higher when the incidence direction varies in the plane formed by the two recording beams. This can be considered as a drawback, since the holograms need tracking if concentration is required during the whole day or the whole year, but it can be an advantage if the element operates only during a part of the day or over one season. If the incidence direction varies in the perpendicular plane, the angular selectivity is lower, so it is possible to eliminate tracking in this direction.

Due to chromatic selectivity, the efficiency of the volume hologram depends on the wavelength. It is high for a bandwidth centered at a wavelength that is determined by the value of refractive index modulation obtained in the recording step and the angle of incidence. If the chromatic selectivity region is tuned so the lens does not diffract infrared, the heating of the cell, one of the main problems of concentration refractive systems, is avoided. Lower cell temperature results in a higher conversion efficiency, and therefore lower cost/watt [8].

For a plane grating, the behavior is the same in all the points of the hologram. In the case of a holographic lens, the efficiency and its angular and chromatic selectivity vary at each point of the hologram. This has to be taken into account if the concentration factor or the distribution of the energy concentrated on the solar cell need to be calculated.

In previous works, a cylindrical holographic lens has been built and experimentally analyzed in terms of its performance as a solar concentrator [8] with tracking in only one direction. In the present study, the behavior of holographic cylindrical lenses as solar concentrators, for a general geometry of the recording beams, is theoretically evaluated. Some authors [9–11] calculate an average efficiency for all points of the hologram, and apply this efficiency to calculate the energy in the image plane. Since the efficiency does not vary linearly along the surface of the hologram, important information about the real energy distribution on the cell is lost in the mean value.

For this reason, a ray tracing algorithm is developed to simulate the performance across the full aperture of the lens that includes geometrical diffraction effects and efficiency calculation of local gratings. The novelty of the present work is the evaluation of the energy carried by each diffracted ray and the propagation of this energy to the plane of the PV cell, obtaining the real energy distribution on the cell.

2. Theoretical model

Kogelnik's Coupled Wave Theory [12] and the approximate scalar theory developed by Syms [13] are used in order to study the most general case of incidence lying outside of the recording plane. A comprehensive union of both models can be found in the work of Lopez *et al.* [14]. In [14], the diffraction efficiency of a pure phase transmission volume hologram for an incident wave with general wave propagation vector (conical diffraction) and a general polarization direction, as are described in the following paragraphs, are obtained.

In the present work, the equations of conical diffraction, calculating the efficiency and the direction of the diffracted light as a function of the directional cosines of the incident wavefront and the propagation vectors of the recording waves are utilized. The directions of

#234591 - $15.00 USD Received 17 Feb 2015; revised 17 Apr 2015; accepted 20 Apr 2015; published 18 May 2015
(C) 2015 OSA

the rays diffracted by the hologram and its energy can be then calculated by means of ray tracing and thus, the energy distribution on the image plane can be estimated.

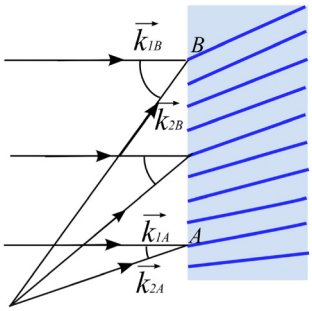

Fig. 1. Recording of a volume and transmission holographic lens.

For this analysis, it is considered that each point of the holographic lens acts as a plane grating ("local grating": Fig. 1). The recording plane of the local grating is defined as the plane that contains the two wave propagation vectors, $\vec{k}_1$ and $\vec{k}_2$, whose interference has created the hologram. The grating vector $\vec{K}$ is determined and it is given by:

$$\vec{K} = \vec{k}_1 \pm \vec{k}_2 \tag{1}$$

For simplicity, only the negative term option from Eq. (1) is considered. This is a good election for volume holograms. As it can be seen from Eq. (2) and (3), $\vec{k}_1$ and $\vec{k}_2$ can be written as a function of their directional cosines inside the material:

$$\vec{k}_1 = \frac{2\pi n}{\lambda_R}(l_1, m_1, n_1) \tag{2}$$

$$\vec{k}_2 = \frac{2\pi n}{\lambda_R}(l_2, m_2, n_2) \tag{3}$$

where n is the refraction index of the holographic material and λ_R is the recording wavelength.

If it is assumed that the hologram media index is sinusoidally modulated and the hologram is a volume one, when it is illuminated with a beam with propagation vector $\vec{k}_o$, there are only two waves that propagate inside the medium: zero order $\vec{k}_o$ and first diffraction order $\vec{k}_i$. The diffracted efficiency of the first order would be maximum when the Bragg condition is fulfilled [Fig. 2(a)]:

$$\vec{k}_i = \vec{k}_o - \vec{K} \tag{4}$$

The diffracted beam is given by the projection of $\vec{k}_i$, $\vec{k}_o$ and $\vec{K}$ on the hologram plane, $z = 0$ [Fig. 2(b)]:

$$\begin{cases} \vec{k}_i \cdot \vec{u}_x = (\vec{k}_o - \vec{K}) \cdot \vec{u}_x \\ \vec{k}_i \cdot \vec{u}_y = (\vec{k}_o - \vec{K}) \cdot \vec{u}_y \end{cases} \tag{5}$$

where $\vec{u}_x$ and $\vec{u}_y$ are the unitary vectors in x and y direction respectively.

#234591 - $15.00 USD Received 17 Feb 2015; revised 17 Apr 2015; accepted 20 Apr 2015; published 18 May 2015
(C) 2015 OSA

Considering Eqs. (1) and (5), the direction cosines (l_i, m_i, n_i) of the diffracted beam $\vec{k}_i$ are given by the following equations [15]:

$$\begin{aligned} l_i &= l_o - \frac{\lambda_R}{\lambda_C}(l_1 - l_2) \\ m_i &= m_o - \frac{\lambda_R}{\lambda_C}(m_1 - m_2) \\ n_i &= \left(1 - l_i^2 - m_i^2\right)^{1/2} \end{aligned} \tag{6}$$

where (l_o, m_o, n_o) are directional cosines of $\vec{k}_o$.

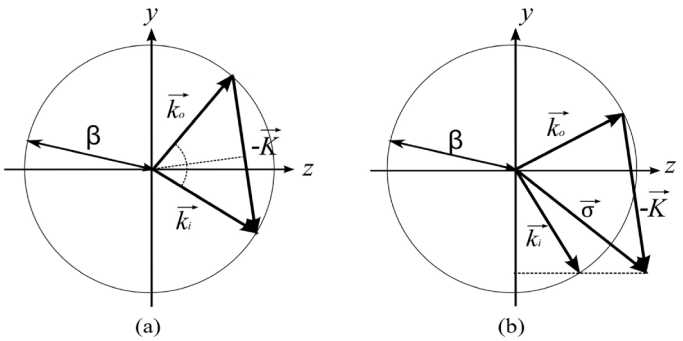

Fig. 2. The vector diagram when Bragg condition is fulfilled (a) or not (b).

The diffractive efficiency for two linear orthogonal polarizations, *N* and *M*, perpendicular and parallel respectively to the plane formed by $\vec{K}$ and $\vec{k}_o$, is given by [14]:

$$\eta_N = \frac{\sin^2\left[\left(\nu^2 + \xi^2\right)^{1/2}\right]}{1 + \frac{\xi^2}{\nu^2}} \tag{7}$$

$$\eta_M = \frac{\sin^2\left[\left(\nu_M^2 + \xi^2\right)^{1/2}\right]}{1 + \frac{\xi^2}{\nu_M^2}} \tag{8}$$

Since solar light is unpolarized, the total diffractive efficiency η_d as the mean of the two contributions η_N and η_M can be considered as:

$$\eta_d = \frac{1}{2}(\eta_N + \eta_M) \tag{9}$$

The parameters ν, ν_M and ξ depend on material characteristics and the deviation of Bragg condition,

$$\nu = \frac{\pi d \Delta n}{\lambda_C (n_o n_i)^{1/2}} \tag{10}$$

$$\nu_M = \nu\left(\vec{k}_o \cdot \vec{k}_i\right) \tag{11}$$

#234591 - $15.00 USD Received 17 Feb 2015; revised 17 Apr 2015; accepted 20 Apr 2015; published 18 May 2015
(C) 2015 OSA

$$\xi = \frac{d\vartheta}{2n_i} \tag{12}$$

where Δn is the index modulation, d the thickness of the holographic medium and λ_C is the wavelength of the incident beam $\vec{k}_o$. Parameter ϑ represents the deviation of the Bragg condition, given by:

$$\vartheta = \frac{\beta^2 - |\vec{\sigma}|^2}{2\beta} \tag{13}$$

where $\beta = \frac{2\pi n}{\lambda_C}$. From Fig. 2(b), $\vec{\sigma} = \vec{k}_o - \vec{K}$; thus, ϑ can be written as a function of the directional cosines of $\vec{k}_o$ and $\vec{K}$:

$$\vartheta = \frac{1}{2}\beta\left(1 - \left[l_o - \frac{\lambda_C}{\lambda_R}(l_1 - l_2)\right]^2 - \left[m_o - \frac{\lambda_C}{\lambda_R}(m_1 - m_2)\right]^2 - \left[n_o - \frac{\lambda_C}{\lambda_R}(n_1 - n_2)\right]^2\right) \tag{14}$$

To reach $\eta_N = 1$, two conditions are necessary: first, Bragg condition must be fulfilled, so $\xi = 0$ $(\vartheta = 0)$; second, $\nu = \frac{\pi}{2}$. The second condition is only possible for a wavelength $\overline{\lambda}_C$ that matches $\Delta n = \frac{2\overline{\lambda_C}(n_o n_i)^{1/2}}{d}$. This value of Δn is determined by the exposure in the recording step, thus the hologram can be tuned to diffract with $\eta_N = 1$ for the desired wavelength [16].

For cylindrical lenses, in which a plane wave and a cylindrical wave interfere, the directional cosines l_1 and l_2 are zero.

3. Experimental measurements

A cylindrical holographic lens in dichromated gelatin emulsion PFG-04 is designed and constructed. The lens is designed for solar concentration applications [8]; thereby, the wavelength for which the efficiency will be maximum as a function of the cell sensitivity can be selected. Since a silicon cell is considered, the central wavelength at the reconstruction will be 800 nm.

The dimensions of the lens and the cell are determined by the desired geometrical concentration factor. In this case, the lens size is 5x5 cm and the cell size is 1x5 cm; thus, the concentration factor is 5 suns.

In Fig. 3, the recording and reconstruction geometry are shown. The recording wavelength is 532 nm and the exposure time is chosen to obtain an index modulation value adequate to give maximum efficiency at 800 nm at the reconstruction [16]. In this way, the chromatic selectivity of the hologram matches the spectral sensitivity curve of silicon PV cells. Given the fact that the central wavelength at the reconstruction is not the same with the recording wavelength, the cylindrical wavefront at the recording is not on axis.

#234591 - $15.00 USD Received 17 Feb 2015; revised 17 Apr 2015; accepted 20 Apr 2015; published 18 May 2015
(C) 2015 OSA

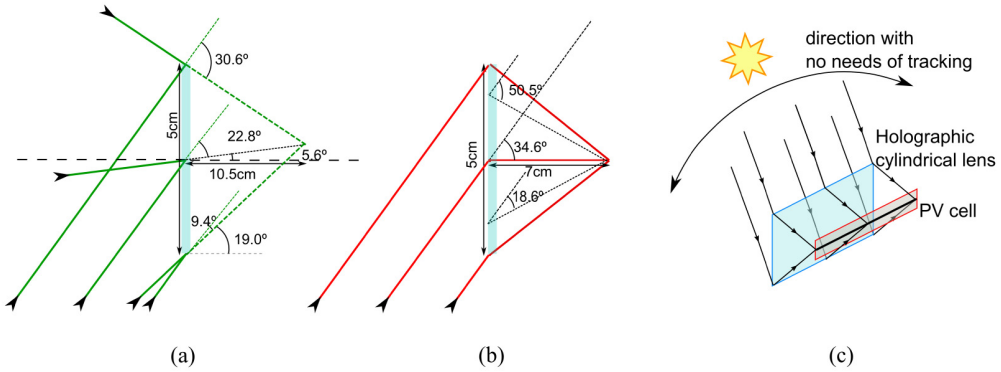

Fig. 3. (a) Recording geometry, (b) reconstruction geometry with monochromatic light and (c) reconstruction geometry with solar light for the cylindrical lens.

The recording interbeam angle has to be large enough to assure the volume condition in all points of the lens. Parameter Q is used to establish the limit of volume regime and it is defined as:

$$Q = \frac{2\pi\lambda_C d}{n\Lambda^2} \tag{15}$$

where Λ is the grating period. If $Q > 2\pi$, the hologram is considered as a volume hologram.

However, angular and chromatic selectivity increase when parameter Q increases; thereby, it is better to adopt a Q value as low as possible. The design criterion for the present work is to obtain efficiency higher than 50% for wavelengths larger than 575 nm at the point of the hologram in which the interbeam angle is lower. From this condition, the recording geometry shown in Fig. 3(a) is determined. The theoretical curve of efficiency, as a function of wavelength at the lower region of the lens depicted in Fig. 3(a), is illustrated in Fig. 4. For wavelengths higher than 575 nm, parameter Q is higher than 2π.

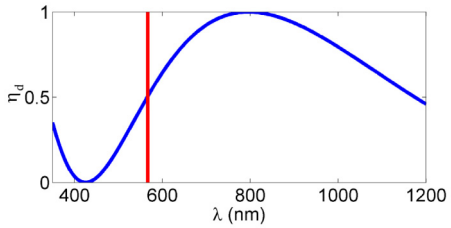

Fig. 4. The efficiency as a function of wavelength in the upper side of the lens shown in Fig. 3.

In Figs. 5(a) and 5(b) the angular selectivity curves in the center of the lens, measured at 800 nm, compared with the corresponding theoretical ones, are plotted. Coordinate θ denotes the variation of incidence direction contained in the recording plane while ϕ indicates the variation of incidence direction in the perpendicular plane. Experimental data have been corrected from reflection and absorption losses in the glass substrate and in the gelatin layer. The maximum diffraction efficiency obtained experimentally is around 95%, close to the theoretical value of 100% for 800 nm. This 5% difference is attributed to index modulation drop, which could be produced at the recording step due to instabilities; anyhow, the index modulation needed for 800 nm is high and the curve of index modulation against exposition saturates around this point [16].

The maximum efficiency peaks are located at 32.1° and –4.1°, instead of 34° and 0°, as it is shown in Fig. 3. This is due to a change of emulsion thickness (shrinkage) occurred during

#234591 - $15.00 USD Received 17 Feb 2015; revised 17 Apr 2015; accepted 20 Apr 2015; published 18 May 2015
(C) 2015 OSA

the wet processing of dichromated gelatin, which changes the direction and module of the grating vector $\vec{K}$. These changes have been included in the theoretical model. The relative difference of FWHM with respect to the theoretical model is 7% and 2.7% in the case of peaks of Fig. 5(a) and 7.6% in the case of Fig. 5(b).

Figure 5(c) illustrates the chromatic selectivity when the hologram is illuminated with white light. The relative difference of FWHM in this case is 3.7%.

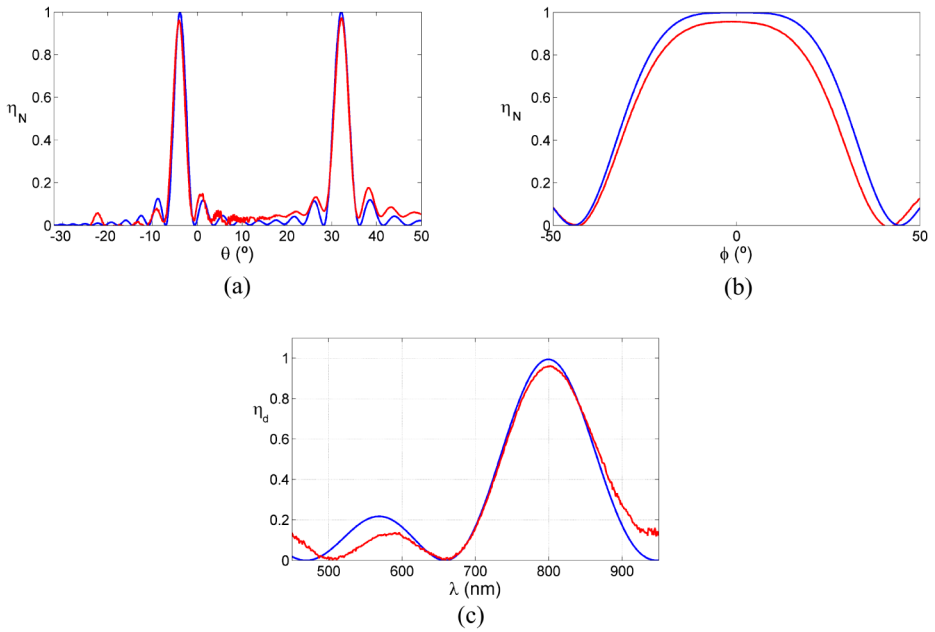

Fig. 5. Experimental (red) and theoretical (blue) curves of the efficiency at 800 nm as a function of (a) the incidence direction θ contained in the recording plane, (b) the incidence direction ϕ perpendicular to the recording plane. (c) Theoretical (blue) and experimental (red) efficiency as a function of wavelength.

4. Influence of recording geometry on the performance of cylindrical holographic lenses

The theoretical model is utilized to analyze the influence of the recording geometry on the angular and chromatic selectivity of holographic solar concentrators. To illustrate the usefulness of the developed algorithm, two typical recording geometries [6, 8] of cylindrical lenses are compared. The first one (lens 1) is the configuration shown in Fig. 3. The recording and reconstruction geometry of the second lens (lens 2) are illustrated in Fig. 6.

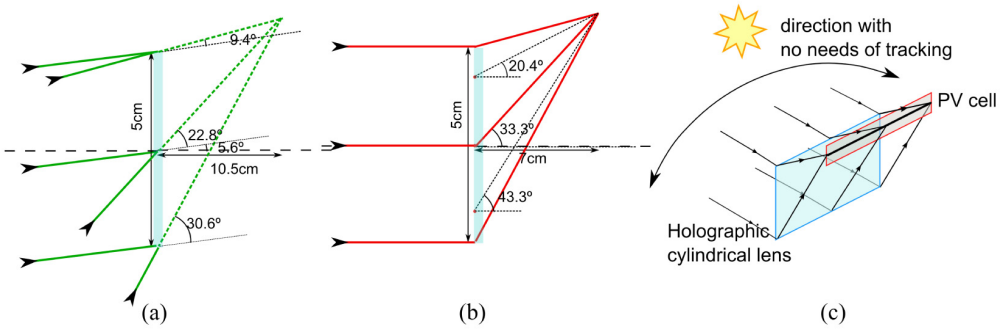

Fig. 6: (a) The recording geometry, (b) the reconstruction geometry with monochromatic light and (c) the reconstruction geometry with solar light of the cylindrical lens.

#234591 - $15.00 USD Received 17 Feb 2015; revised 17 Apr 2015; accepted 20 Apr 2015; published 18 May 2015
(C) 2015 OSA

In lens 1 the cylindrical wavefront is reconstructed on-axis while in lens 2, the cylindrical wavefront is reconstructed off-axis. In the recording step, the interbeam angle at the center of the plate is the same for both lenses, but local gratings are not equal, so the lenses would have different chromatic and angular selectivity.

4.1 Local analysis

In Fig. 7, the monochromatic efficiency (at 800 nm) as a function of the incidence angle at three different points of each lens: at the upper side (+20 mm from the center), at the center and at the bottom (–20 mm from the center) is illustrated.

Lens 2 maintains better efficiency for a larger range of ϕ angles in comparison with lens 1; thereby, lens 2 is expected to have a better behavior if the tracking in ϕ direction is eliminated.

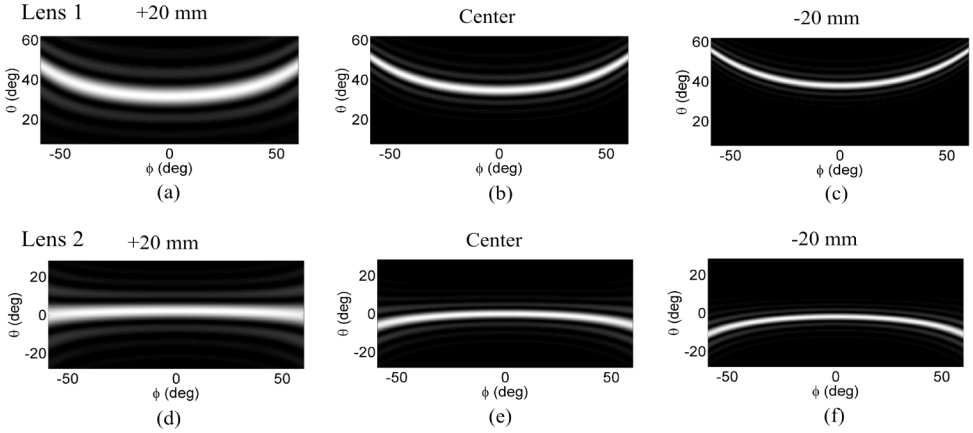

Fig. 7. The efficiency as a function of the incidence angle θ and ϕ in lens 1 and lens 2, calculated at three points of the lenses: at the center, (b) and (e); 20 mm above the center, (a) and (d); and 20 mm below the center, (c) and (f). Values range from black (η = 0) to white (η = 1).

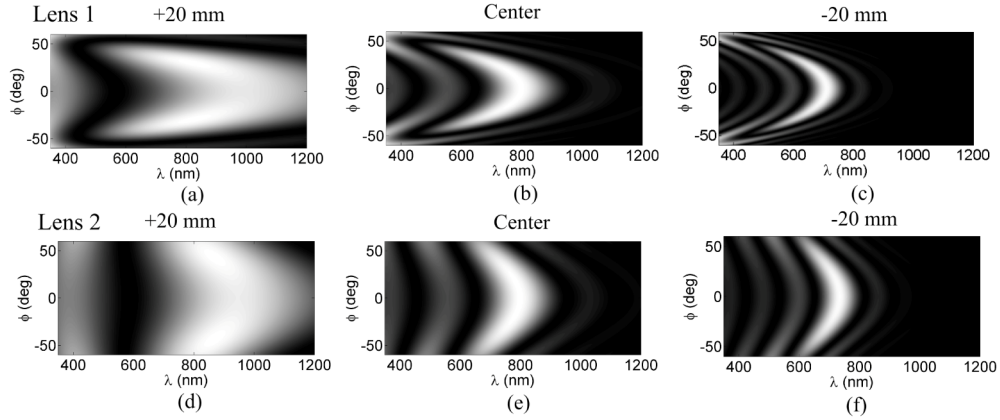

Fig. 8. The efficiency as a function of the incidence angle ϕ and λ in lens 1 and lens 2 calculated at three points of the lenses: at the center (b) and (e), 20 mm above the center (a) and (d), and 20 mm below the center (c) and (f). Values range from black (η = 0) to white (η = 1).

It should be taken into account the fact that these graphics are calculated for 800 nm; thus, although the efficiency drops in some points, for other wavelengths the efficiency would be

#234591 - $15.00 USD Received 17 Feb 2015; revised 17 Apr 2015; accepted 20 Apr 2015; published 18 May 2015
(C) 2015 OSA

maximum. This effect can be observed in Fig. 8 where the efficiency as a function of wavelength and ϕ is presented. In the frame of attending the chromatic selectivity, both lenses are very similar.

4.2 Global analysis

As it has been demonstrated, the efficiency strongly depends on the point of the lens; thereby, it is necessary to make a global analysis taking into account the whole aperture.

By means of the present ray tracing calculation, the spot diagram considering the diffracted rays for each lens at the cell plane (Fig. 9) for three different wavelengths (700, 800 and 900 nm) is evaluated, when the direction of the incident beam fulfills the Bragg condition for 800 nm.

Both lenses present chromatic dispersion in y-direction (in the case of lens 2 the dispersion is higher than in lens 1); thereby not all the rays reach the cell area. This fact will reduce the theoretical geometrical concentration.

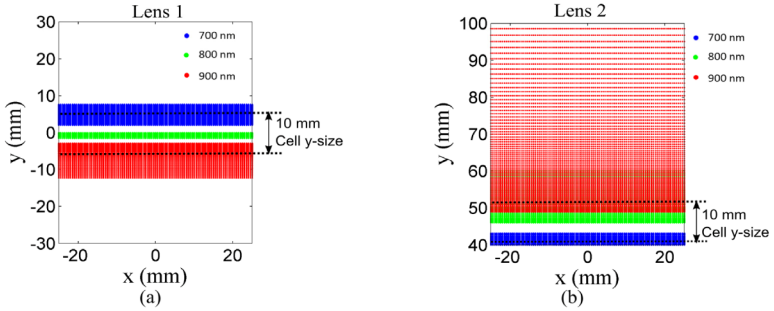

Fig. 9. Spot diagrams at the cell plane of lens 1 (a) and lens 2 (b) for 700, 800 and 900 nm.

Spot diagrams of Fig. 9 give information about the geometrical behavior of the lenses, but do not reveal the energy that reaches the cell, since each ray transports different energy depending on its wavelength and its incidence point on the lens.

Thus, to analyze the optical efficiency of the concentrator, it is necessary to calculate the light energy that reaches the cell area. From this energy, a set of optical concentration coefficients [17] are calculated as follows:

The cell area, A_c, is divided into small areas, ΔA_c. The local spectral optical concentration ratio, $\eta_{\lambda,y}$, in y-direction is given by:

$$\eta_{\lambda,y} = \frac{\Phi_{2,\lambda,y}}{\Phi_{1,\lambda}} \frac{A_L}{\Delta A_c} \tag{16}$$

where $\Phi_{1,\lambda}$ is the radiative spectral energy at the entrance pupil area, A_L, and $\Phi_{2,\lambda,y}$ is the radiative spectral energy that reaches ΔA_c.

Figure 10 shows the results obtained for both lenses.

#234591 - $15.00 USD Received 17 Feb 2015; revised 17 Apr 2015; accepted 20 Apr 2015; published 18 May 2015
(C) 2015 OSA

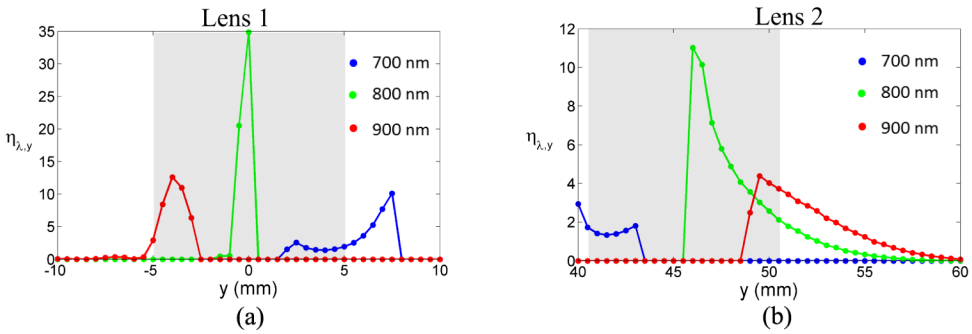

Fig. 10. Local spectral optical concentration ratio as a function of the *y*-coordinate in cell plane for (a) lens 1 and (b) lens 2.The shadow zone corresponds to cell width.

By focusing on the maximum values obtained in each lens, it can be observed that lens 1 concentrates more energy of the three wavelengths; nevertheless, in the case of lens 2, the energy is more distributed over the cell.

Integrating in a range of wavelengths, the local optical concentration ratio in y-direction, η_y, is given by:

$$\eta_y = \frac{\Phi_{2,y}}{\Phi_1}\frac{A_L}{\Delta A_c} \tag{17}$$

where Φ_1 is the radiative energy at the entrance pupil area and $\Phi_{2,y}$ is the radiative energy of the rays that reach ΔA_c in that range of wavelengths.

The results are shown in Fig. 11, for a range of wavelengths from 650 nm to 950 nm. This range is selected as a function of the sensitivity curve of the cell. It can be observed that lens 1 concentrates the light slightly more than lens 2.

In Figs. 10 and 11, it is considered that the energy associated with each ray at the entrance pupil does not depend on the wavelength and the reflection and absorption losses on the glass substrate are not taken into account.

For the full cell area, the optical concentration ratio is given by:

$$\eta = \frac{\Phi_2}{\Phi_1}\frac{A_L}{A_c} \tag{18}$$

where Φ_2 is the radiative energy at the cell area. The optical concentration ratio η is 1.94 for lens 1 and 1.67 for lens 2.

#234591 - $15.00 USD Received 17 Feb 2015; revised 17 Apr 2015; accepted 20 Apr 2015; published 18 May 2015
(C) 2015 OSA

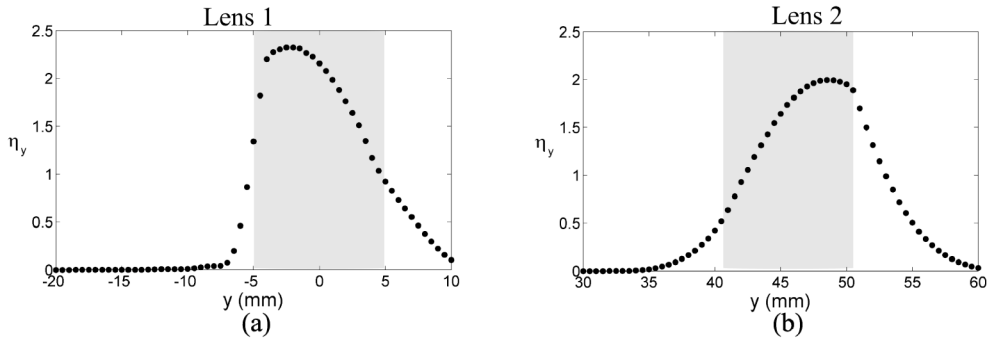

Fig. 11. Local optical concentration ratio as a function of the *y*-coordinate in cell plane for (a) lens 1 and (b) lens 2, considering wavelengths from 650 nm to 950 nm.The shadow zone corresponds to cell width.

Both lenses presents an optical efficiency lower than 40%, mainly due to chromatic dispersion, aberration effects and light diffracted in zero order. On the other hand, holographic concentrators have the advantage that the infrared radiation is not concentrated, avoiding cell overheating and enhancing the cell conversion efficiency. If the optical efficiency is improved by optimizing the recording geometry, holographic concentrators will be an attractive option to refractive concentrators.

5. Conclusions

A ray tracing algorithm has been developed in order to analyze the energy performance of volume and transmission holographic lenses as solar concentrators.

The algorithm is a powerful simulation tool that allows analyzing different designs of holographic concentrators, conducting a local analysis of angular and chromatic selectivity in different points of the lens, and performing a global analysis, by means of spots diagrams and energy integration onto cell, taking into account the whole aperture of the lens.

A holographic element was constructed in order to validate the model for a specific set of designed parameter. The comparison demonstrated very good agreement for both, chromatic and angular selectivity.

Two lens configurations with on-axis (lens 1) and off-axis (lens 2) cylindrical wave reconstructions are analyzed. Lens 2 has a better performance when the incident light goes out of the Bragg condition, as it can be seen in Fig. 7, but this lens presents a higher chromatic dispersion. An integration process of ray energy along the cell is conducted in order to obtain the optical concentration ratio when the incident beam fulfills the Bragg condition for 800 nm. Lens 1 shows an average concentration ratio of 1.94, which is 16.1% higher than in lens 2. A comparison of total concentration ratio when incident beam varies along the day will be necessary to determine the best configuration. As the theoretical model can be used to calculate the concentration ratio for any direction of the incident beam, this would be the purpose of future work.

Acknowledgments

This research has been supported by the Spanish Ministerio de Economía y Competitividad (grants FIS2012-35433 and ENE2013-48325-R), the Diputación General de Aragón (Grupo Consolidado TOL, T76) and the Generalitat de Catalunya (grant FI-DGR 2015).

In memoriam of Prof. Dr. Manuel Quintanilla.